The Astrophysical Journal, 676:137–146, 2008 March 20

FIRST DETECTION OF ^{12}CO(1 → 0) EMISSION FROM TWO NARROW-LINE SEYFERT 1 GALAXIES

Toshihiro Kawaguchi,[1] Kouichiro Nakanishi,[2] Kotaro Kohno,[3] Kouji Ohta,[4] and Kentaro Aoki[5]
Received 2007 September 14; accepted 2007 December 5

ABSTRACT

In order to investigate how the growth of galactic bulges progresses with the growth of central black holes (BHs), we observed molecular gas (fuel for the coming star formation) in possibly young active galaxies: narrow-line Seyfert 1 galaxies (NLS1s). We present the results of radio observations of ^{12}CO(1 → 0) using the Nobeyama Millimeter Array (with 2–4 kpc spatial resolution) for two FIR-bright NLS1s, yielding the first detection of their CO emission. Corresponding molecular gas masses $M(\mathrm{H_2})$ of (1–3) $\times 10^9$ $M_\odot$ are the second and fourth largest among NLS1s. By estimating dynamical masses and bulge masses M_{bulge} for these two NLS1s using CO channel maps and CO line widths, we found that $M(\mathrm{H_2})$ amounted to 13%–35% of these masses. Taking into account the star formation efficiency ($\sim$0.1), the increase in M_{bulge} in those NLS1s in the near future ($\lesssim 10^{7.5}$ yr) is not expected to be a huge fraction (1%–5% of the preexisting stars). Bulge growth may have finished before BH growth, or bulge-BH coevolution may proceed with many occasionally discrete events, where one coevolution event produces only a small amount of mass growth of BHs and bulges. We also discuss the ratios of star formation rate to gas accretion rate onto BHs, finding that two NLS1s have very small ratios ($\approx$1) compared with the $M_{\mathrm{bulge}}/M_{\mathrm{BH}}$ ratios found in active and inactive galaxies ($\approx$700). This huge difference suggests either nonoverlapped coevolution, a long star formation duration, or a temporarily high accretion rate during the NLS1 phase.

Subject headings: galaxies: active — galaxies: evolution — galaxies: individual (IRAS 04312+4008, IRAS 05262+4432) — ISM: molecules — radio lines: ISM

Online material: color figures

1. INTRODUCTION

The mass of the galactic spheroid component (the galactic bulge or elliptical galaxy itself) is tightly correlated with the mass of the central black hole (BH) in both normal and active galaxies (Gebhardt et al. 2000; Ferrarese & Merritt 2000; Nelson 2000). Along with the lack of cosmic evolution (Shields et al. 2003; Kiuchi et al. 2006; but also see Akiyama 2005; Woo et al. 2006; Borys et al. 2005), the tightness of the correlation indicates that the growth of the spheroid mass and of the BH mass (M_{BH}) occurs almost simultaneously.

However, no direct evidence for simultaneous coevolution has been found, and thus its physical origin remains a great mystery. Jet and/or outflow from an active galactic nucleus (AGN) may govern the formation of the spheroid (Silk & Rees 1998), i.e., BHs made before the growth of the bulges. On the contrary, radiation drag by massive stars during bulge formation may have controlled BH growth (Umemura 2001), resulting in bulges formed prior to the growth of the BHs.

Most numerical studies presume that cool, interstellar gas drives coevolution (e.g., Kauffmann & Haehnelt 2000). For instance, semianalytical approaches assume that a major merging of galaxies initiates the growth of BHs and bulges, and they usually adopt an AGN duration (*e*-folding accretion timescale) of around $10^{7.5}$ yr and a star formation duration of $\sim 10^8$ yr (Kauffmann et al. 1993; Kauffmann & Haehnelt 2000). Theoretically and observationally, it is unknown which growth phase precedes another. Now let us simply assume that the BH and bulge growth phases begin in conjunction and proceed with similar durations. Then we will see enough molecular gas—fuel for the coming star formation—in the bulges of AGNs in the early stage of BH growth (e.g., in the first quarter of the AGN/star formation durations). Old AGNs (e.g., in the last quarter of the durations) that have existed for a long time since the ignition of coevolution would have already consumed the gas through the past star formation, with only a tiny amount left over for further bulge growth.

Here we note a subsample of AGNs, narrow-line Seyfert 1 galaxies (NLS1s), as possibly young AGNs. NLS1s are characterized (see Pogge 2000) by the following: (1) They have narrower Balmer lines of hydrogen (FWHM of H$\beta \leq 2000$ km s^{-1}) relative to the usual broad-line Seyfert 1 galaxies (BLS1s) and QSOs with a FWHM of H$\beta \gtrsim 5000$ km s^{-1} (Osterbrock & Pogge 1985). (2) They often emit strong optical Fe II multiplets (e.g., Halpern & Oke 1987). (3) They often show steep and luminous soft X-ray excess (Pounds et al. 1995; Otani et al. 1996; Boller et al. 1996; Wang et al. 1996; Laor et al. 1997; Leighly 1999b). (4) They show rapid X-ray variability (Otani et al. 1996; Boller et al. 1997; Leighly 1999a; Hayashida 2000). Characteristics (2)–(4) indicate that NLS1s are nonobscured objects, unlike type 2 (i.e., obscured) AGNs. Currently, the most promising picture of NLS1s is that they contain relatively less massive BHs (with $M_{\mathrm{BH}} \sim 10^6$–$10^8$ $M_\odot$) and higher L/L_{Edd} ratios ($\sim$1; e.g., Brandt & Boller 1998; Hayashida 2000; Mineshige et al. 2000), where L and L_{Edd} are the AGN luminosity and Eddington luminosity, respectively. NLS1s occupy 10%–30% of type 1 AGNs in the local universe (see Kawaguchi et al. 2004a).

High L/L_{Edd} ratios of NLS1s imply that their BHs are growing rapidly via super-Eddington accretion (Rees 1992; Mathur 2000; Kawaguchi et al. 2004a). Provided that a gas accretion rate onto the central BH, $\dot{M}$, during an AGN phase does not drastically

[1] Department of Physics and Mathematics, Aoyama Gakuin University, Sagamihara, Kanagawa 229-8558, Japan; kawaguti@phys.aoyama.ac.jp.
[2] Nobeyama Radio Observatory, Minamimaki, Minamisaku, Nagano 384-1305, Japan.
[3] Institute of Astronomy, University of Tokyo, Mitaka, Tokyo 181-0015, Japan.
[4] Department of Astronomy, Kyoto University, Kyoto 606-8502, Japan.
[5] Subaru Telescope, National Astronomical Observatory of Japan, 650 North A'ohoku Place, Hilo, HI 96720.

change with time (see Collin & Kawaguchi 2004), large $\dot{M}/M_{\rm BH}$ ratios of NLS1s also mean that the elapsed time since the ignition of AGN activity is shorter than that of BLS1s. (If the gas accretion lasts long enough, then $M_{\rm BH}$ will not be so small.) The bulge luminosities of NLS1s are smaller than those of BLS1s, in general (Botte et al. 2004).

NLS1s are likely young AGNs (during the first 10%–30% of the whole AGN lifetime [$\sim 10^8$ yr; see § 6]) in the process of coevolution of supermassive BHs and bulges. This is our working hypothesis in this study. We consider them to be unique and the best targets for exploring how the BH-bulge coevolution proceeds. If the growth phases of BHs and bulges are really overlapped, the bulges of NLS1s may also be rapidly growing with a significant amount of molecular gas accumulated in their bulges. Do they show large ratios of molecular gas to bulge masses, compared with BLS1s (which are expected to be older than NLS1s, based on their lower $\dot{M}/M_{\rm BH}$ ratios)? To examine these conjectures, we need copious data for numerous NLS1s, collected under the condition that the spatial resolution is less than the bulge size (typically on the order of 1 kpc).

However, NLS1s are rare among Seyfert 1 galaxies, and thus we do not have many NLS1s with detected CO emission in the nearby universe. Therefore, observations to increase the number of CO-detected NLS1s are fundamental for listing strong CO emitters, with an eye to follow-up subkiloparsec observations of them. The $M_{\rm BH}$-bulge mass relation of NLS1s and its comparison with the relation of inactive galaxies are subjects of debate (Komossa & Xu 2007 and references therein). Our observations would also help to clarify whether NLS1s are really young AGNs.

In this paper we present the observational results of the ^{12}CO($1 \rightarrow 0$) line from two NLS1s with $5''$–$6''$ (2–4 kpc at their distance) spatial resolution using the Nobeyama Millimeter Array (NMA) at the Nobeyama Radio Observatory (NRO). The next section outlines the target selection, and § 3 describes the log and data reduction of our radio observations. We then show the results in § 4, followed by discussions on bulge-to-gas mass ratios in § 5. The final section is devoted to discussion and summary. The cosmological parameters adopted in this paper are $H_0 = 70$ km s^{-1} Mpc^{-1}, $\Omega_M = 0.3$, and $\Omega_\Lambda = 0.7$.

2. SELECTION OF TARGETS

So far, there are only a few NLS1s whose CO lines are detected in the nearby universe. Intending to increase the number of such NLS1s, we thus carried out the following observations (with beam size $\sim 6''$) onto two NLS1s with no CO observations reported.

In order to select targets, we investigated flux densities at 100 μm (measured with *IRAS*), which roughly trace the CO line flux (Solomon et al. 1997), for all NLS1s at declination $> -25°$ and redshift $z \leq 0.067$ (the sample summarized by Ohta et al. 2007).

In NGC 4051, which has the largest 100 μm flux (24 Jy), the CO emission line is clearly detected (Young et al. 1995; Maiolino et al. 1997; Kohno et al. 1999a, 1999b), whereas only an upper limit is obtained for the second-brightest 100 μm (4.7 Jy) object (Mrk 766 = NGC 4253), with $M({\rm H_2}) < 10^{7.7}\ M_\odot$ (Taniguchi et al. 1990). It then turns out that the third- and fourth-brightest NLS1s ($\sim$4 Jy) have no radio observations made of their molecular gas. We select these two SBb galaxies, IRAS 04312+4008 ($z = 0.020$) and IRAS 05262+4432 ($z = 0.032$), to observe.

We regard these two NLS1s as the best targets to elucidate how bulge growth is accompanied by BH growth. By assuming a virialized broad-line region (Wandel et al. 1999; Kaspi et al. 2000), $M_{\rm BH}$ is estimated with Hβ width as follows:

$$M_{\rm BH} = 4.82 \times 10^6\ M_\odot \left[\frac{{\rm FWHM(H\beta)}}{1000\ {\rm km\ s^{-1}}}\right]^2 \left[\frac{\nu L_\nu(5100\ {\rm \AA})}{10^{44}\ {\rm erg\ s^{-1}}}\right]^{0.7}. \quad (1)$$

Although some improved equations in place of the equation above are suggested by, e.g., Onken et al. (2004), Kaspi et al. (2005), and Collin et al. (2006), we adopt equation (1) in this paper for simplicity. The FWHM(Hβ), optical luminosity, and estimated BH masses for the two objects are 860 km s^{-1}, $10^{44.6}$ erg s^{-1}, and $10^{7.0}\ M_\odot$ and 740 km s^{-1}, $10^{45.2}$ erg s^{-1}, and $10^{7.3}\ M_\odot$ for IRAS 04312 and IRAS 05262, respectively (Ohta et al. 2007). Based on the $M_{\rm BH}$ estimations in this way and our spectral models for $\dot{M}$ evaluation (Kawaguchi 2003), they have extremely small $M_{\rm BH}/\dot{M}$ ratios (<2 Myr) even among NLS1s (all CO data for NLS1s taken from our observations and from the literature will be given in a forthcoming paper [T. Kawaguchi et al., in preparation]). Thus, little time has probably passed since each BH began to grow.

TABLE 1
LOG OF OBSERVATIONS

Target	Redshift	Integration Time (hr)	Beam Size (arcsec)	Scale (kpc arcsec^{-1})
IRAS 04312.......	0.020	6.6	5.8×5.2	0.40
IRAS 05262.......	0.032	7.7	6.1×5.2	0.63

3. OBSERVATION AND DATA REDUCTION

In 2006 April–March, aperture synthesis observations toward two NLS1s were carried out with the NMA D configuration, with the longest baseline of 82 m. The beam size ($\sim 5'' \times 6''$) corresponds to 2–4 kpc at their distances (see § 5 for their bulge effective radii). The NMA consists of six 10 m antennas, although one antenna was sometimes out of order during our observations.

In all observations, we searched for CO($1 \rightarrow 0$) ($\lambda_{\rm rest} = 2.6008$ mm or $\nu_{\rm rest} = 115.271$ GHz) lines by setting the central frequency of each observation to the redshifted frequency. The back end we used was the Ultra-wide Band Correlator (UWBC; Okumura et al. 2000), which was set to cover 512 MHz ($\sim$1300 km s^{-1}) with 256 channels at 2 MHz resolution (with $\sim$10 km s^{-1} effective resolution after the Hanning window function was applied). The quasar 3C 111 was used for phase and amplitude reference calibrations, while 3C 454.3 was used for bandpass calibration. Total on-source integration time on each object and the beam size are summarized in Table 1. To calibrate absolute flux scale, Uranus was used. The uncertainty in the absolute flux scale is typically $\sim$10%. Standard data reduction was performed using the UVPROC-II software package developed at NRO (Tsutsumi et al. 1997). Some parts of the data taken under bad radio seeing conditions were removed from our analysis. After clipping a small fraction of data with unusually high amplitude, the data were imaged with natural UV weighting and CLEANed with the NRAO AIPS package. The absolute positional accuracy is less than $\sim$5% of the beam size.

4. RESULTS

The CO emission from the two *IRAS* galaxies was detected, for the first time, by our observations.

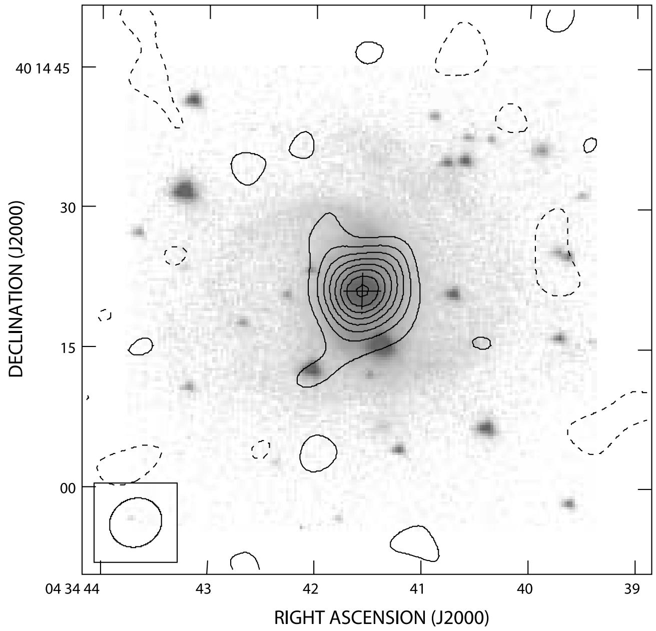

FIG. 1.—CLEANed contour map of the CO(1 → 0) emission line from IRAS 04312 binned in frequency over 320 km s^{-1}, on top of the optical image (Ohta et al. 2007). Contour levels show −2, 2, 4, . . ., 14, and 16 σ, with 1 σ = 2.0 Jy beam^{-1} km s^{-1}. The $4'' \times 4''$ cross represents the peak position of the CO distribution. In the bottom left corner, the beam size ($5.8'' \times 5.2''$) is shown. [*See the electronic edition of the Journal for a color version of this figure.*]

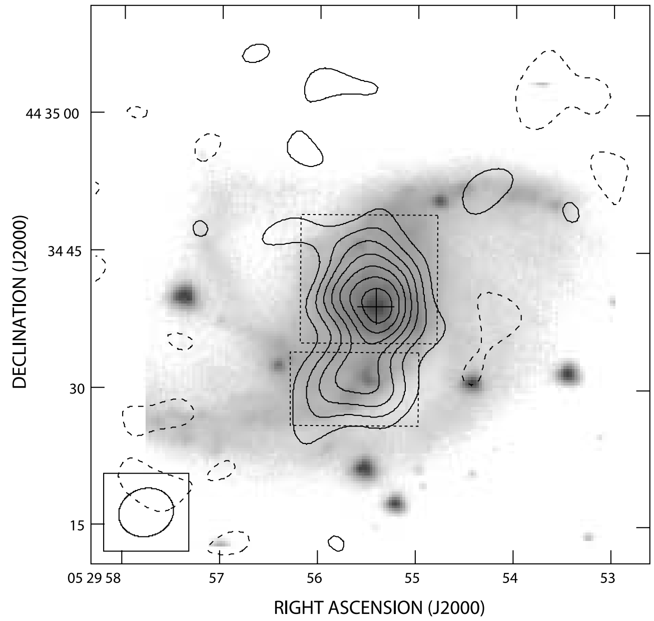

FIG. 2.—Same as Fig. 1, but for IRAS 05262. A large square at the galactic center and another square south of the center indicate the areas over which the spectra (Fig. 4) are integrated. The contour map shows the CO emission integrated over 190 km s^{-1}, with 1 σ = 1.2 Jy beam^{-1} km s^{-1}. The beam size is $6.1'' \times 5.2''$. [*See the electronic edition of the Journal for a color version of this figure.*]

4.1. *Distribution of Gas*

To show the distribution of the molecular gas of the two targets, we show here the CLEANed maps binned over broad velocity ranges (320 or 190 km s^{-1}) in Figures 1 and 2. Throughout, north is at the top and east to the left. The ranges integrated are shown in Figures 3 and 4 and labeled "map." In both objects, the peak flux densities amount to up to $\sim$16 σ ($\sim$100 mJy beam^{-1}). By looking at the 2MASS images, we find that the peak of CO emission from each galaxy coincides with the peak position of the NIR emission of each galaxy. The peak position of the CO emission is marked with a cross. The cross also appears in the channel maps (Figs. 5 and 6) in order to show the central position. Optical images taken at the University of Hawaii 88 inch (2.2 m) telescope at the *I* band with $\sim 0.6''$ (FWHM) image quality (Ohta et al. 2007) are also shown to present the morphology of the host galaxies.

The gas distribution of IRAS 04312 is quite centrally concentrated (Fig. 1). The FWHM of this signal is about $7.2'' \times 6.8''$. Considering the beam size ($5.8'' \times 5.2''$), the spatial extent (in diameter) of the gas is estimated to be $\sim 4.3'' \times 4.4''$ ($\sim$1.7–1.8 kpc), much smaller than the beam. On the other hand, the molecular gas of IRAS 05262 (Fig. 2) seems larger than the beam size ($6.1'' \times 5.2''$). The FWHM of its central CO emission, $\sim 8.3'' \times 10.7''$, suggests that the actual size is $\sim 5.6'' \times 9.4''$ (3.5×5.9 kpc), elongated in the north-south direction. In § 5 these sizes are compared with their bulge effective radii, estimated by a couple of methods, to discuss how much of the detected CO gas is located within the bulge.

Incidentally, isolated CO emission is seen $\sim 7''$ ($\sim$4.4 kpc in projected distance) south of the center of IRAS 05262, which seems to arise from a star-forming region evident in the optical image.

4.2. CO *Spectra and Molecular Gas Masses*

Next, we present spectra of the CO(1 → 0) line for the two NLS1s in Figures 3 (IRAS 04312) and 4 (IRAS 05262). The spectrum of each central region shows a double-horned shape, indicating a rotating molecular disk origin. The horizontal solid lines, labeled "map," show the ranges used in Figures 1 and 2 to draw the frequency-integrated maps. The arrows indicate the recession velocity of the targets.

The CO-to-H_2 conversion factor is estimated to be 0.8 and 2.9 $M_\odot$ (K km s^{-1} pc^2)$^{-1}$ for ultraluminous infrared galaxies (Downes & Solomon 1998) and for our Galaxy (Dame et al. 2001), respectively. When converting CO line flux to H_2 mass, $M(H_2)$, the conversion factor 1 $M_\odot$ (K km s^{-1} pc^2)$^{-1}$ is assumed throughout this paper. The same conversion factor is applied for recomputations of $M(H_2)$ for objects taken from the literature.

The velocity-integrated flux from IRAS 04312, measured over the same area used to draw Figure 3, is 57 ± 3 Jy km s^{-1}, meaning that $M(H_2) = (1.0 \pm 0.05) \times 10^9\ M_\odot$. The velocity integration range is shown in Figure 3 and labeled "flux," while the velocity-integrated flux from the central region of IRAS 05262, measured in the box including the CO peak (Fig. 2), is 62 ± 3 Jy km s^{-1}, corresponding to $M(H_2)$ of $(2.8 \pm 0.1) \times 10^9\ M_\odot$. These molecular gas masses are the second and fourth largest masses (to the best of our knowledge) among NLS1s, with I Zw 1 [$M(H_2) = 10^{9.5}\ M_\odot$ and $z = 0.061$; Maiolino et al. 1997] and PG 1440+356 [$M(H_2) = 10^{9.3}\ M_\odot$ and $z = 0.079$; Evans et al. 2001] being the first and third ones. A summary of all NLS1s whose CO emission is detected will be given in a forthcoming paper (T. Kawaguchi et al., in preparation). If we restrict ourselves to $z \leq 0.05$ (where $1''$ angular resolution is equivalent to 1 kpc spatial resolution), these masses are the largest among NLS1s.

In Figure 4 (*bottom*), the spectrum of the isolated CO emission ($\sim 7''$ south of the center) is also shown. This quite narrow emission line has a velocity-integrated flux of 21 ± 1.4 Jy km s^{-1}, corresponding to $M(H_2) = (9.3 \pm 0.6) \times 10^8\ M_\odot$. Translating this H_2 mass into a star formation rate (SFR) by using equations (5) and (6), shown later, we get an SFR of 3.0 $M_\odot$ yr^{-1}.

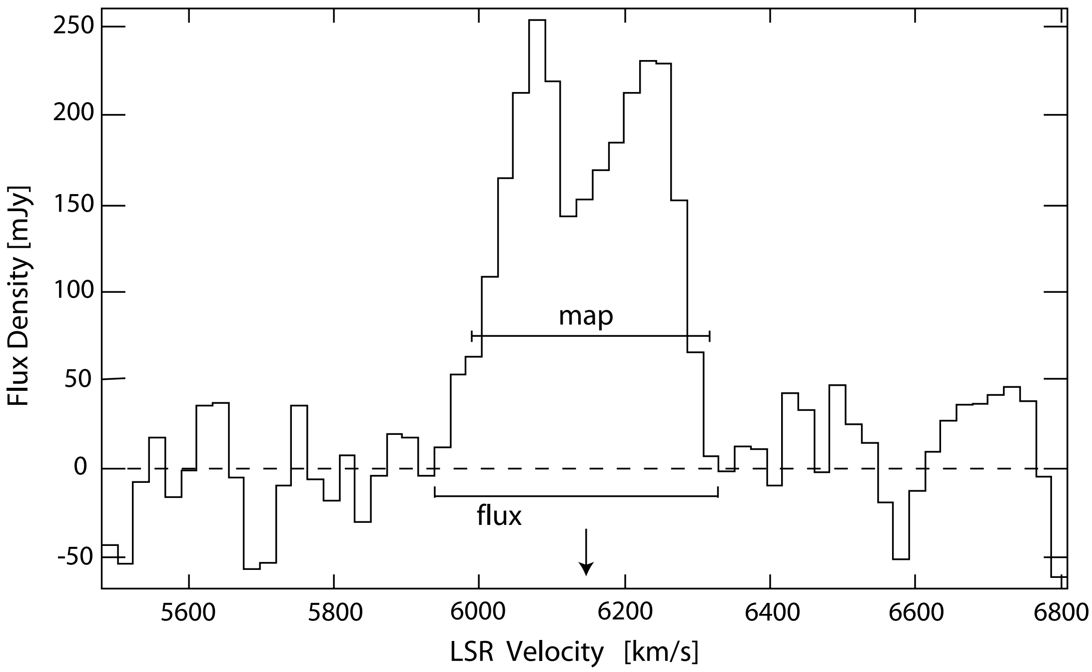

FIG. 3.—CO(1 → 0) spectrum of the central region of IRAS 04312, integrated over a $12'' \times 12''$ box centered on the peak of the CO emission. (Hereafter, velocity notation is based on optical convention.) The bin width and frequency step are the same as those for the channel maps (Fig. 5). The arrow indicates the recession velocity of the galaxy, measured with H I gas (Paturel et al. 2003). The horizontal line labeled "map" indicates the range used in Fig. 1 to draw the frequency-integrated map. The horizontal line labeled "flux" indicates the range for measuring the velocity-integrated flux.

4.3. *Kinematics*

Figures 5 and 6 show channel maps of the two *IRAS* galaxies. Each map is binned over 42 km s^{-1}, and the velocity step between adjacent maps is 21 km s^{-1}. The cross in each panel represents the peak position of the full CO emission (Figs. 1 and 2). In IRAS 05262, a molecular gas clump at $\sim 7''$ south of the center is evident.

In both objects, rotating dynamics around each center (*cross*) is clearly seen. Position-velocity diagrams shown in Figures 7 and 8 also indicate rotation. The position angle used for each diagram is determined as follows. Two panels (of high signal-to-noise ratio peaks) are chosen from each channel map. Then the peak positions in the two maps (with two channels separated by $\sim$210 km s^{-1}) are connected by a line.

Next, we derive dynamical mass (i.e., enclosed mass) $M_{\rm dyn}$ from these position-velocity diagrams. We estimate an inclination angle i for each galaxy by measuring the ellipticity of the *I*-band image (Ohta et al. 2007), where the inclination angle of 0° means a face-on view of a rotating CO gas disk: $i = 40° \pm 1°$ (IRAS 04312) and $i = 53° \pm 5°$ (IRAS 05262). Then the dynamical mass is evaluated as

$$M_{\rm dyn} = 5.8 \times 10^8\ M_\odot \left(\frac{\Delta V}{100\ {\rm km\ s^{-1}}}\right)^2 \left(\frac{R}{\rm kpc}\right) (\sin i)^{-2}, \quad (2)$$

where ΔV and R are the velocity difference and the separation. Positional separations R and velocity differences ΔV between two peaks in the position-velocity diagrams are $2.7''$ (1.1 kpc in projected distance) and 164 km s^{-1} for IRAS 04312 and $5.1''$ (3.2 kpc) and 165 km s^{-1} for IRAS 05262. The enclosed mass $M_{\rm dyn}$ within the central region of IRAS 04312 is $4.1 \times 10^9\ M_\odot$, while for IRAS 05262 $M_{\rm dyn} = 8.0 \times 10^9\ M_\odot$. The peak-to-peak separations represent the lower limits of their CO gas sizes. As we see in § 4.1, the CO gas in IRAS 04312 is indeed more concentrated than that in IRAS 05262.

5. SIZES OF CO GAS AND BULGE

Here we discuss the extent of the CO gas in two NLS1s (§§ 4.1 and 4.3) and compare it with their bulge sizes. The spatial extent (in diameter) of the CO gas in IRAS 04312 is estimated to be $\sim 4.3'' \times 4.4''$ ($\sim$1.7–1.8 kpc). On the other hand, IRAS 05262 seems to have extended and elongated CO gas at its center with a size of $\sim 5.6'' \times 9.4''$ (3.5×5.9 kpc). The peak-to-peak separations in the position-velocity diagrams (Figs. 7 and 8), $2.7''$ (1.1 kpc) and $5.1''$ (3.2 kpc) for IRAS 04312 and IRAS 05262, respectively, also indicate that the molecular gas of IRAS 05262 is more extended than that of IRAS 04312.

Now let us estimate the bulge effective radius ($R_{\rm eff}$) from the [O III] width as follows. The FWHM of the [O III] emission lines of IRAS 04312 is 380 km s^{-1} (Véron-Cetty et al. 2001). Since the [O III] widths and velocity dispersions (σ_*) are nearly the same (Heckman et al. 1989; Nelson & Whittle 1996), the σ_* for this object is evaluated to be about 160 km s^{-1} by dividing the [O III] FWHM width by 2.35. Elliptical galaxies and bulges of disk galaxies obey a canonical relation about their dynamics, size, etc. (the fundamental plane). The velocity dispersion can be translated into the size as follows (Guzman et al. 1993):

$$R_{\rm eff} = 0.56\ {\rm kpc} \left(\frac{\sigma_*}{100\ {\rm km\ s^{-1}}}\right)^{3.15}. \quad (3)$$

Thus, the bulge effective radius of IRAS 04312 is estimated to be about 2.6 kpc or $6.4''$ at its distance. However, the inferred bulge size ($13''$ in diameter) is comparable to the length of the bar seen in the optical image in the north-south direction. Therefore, this method likely overestimates $R_{\rm eff}$ for this object. Adopting the same method for IRAS 05262 by taking its [O III] width (365 km s^{-1}) from Véron-Cetty et al. (2001), its $R_{\rm eff}$ is about 2.3 kpc or $3.6''$ at its distance.

We note that there is a large scatter about the regression equation (eq. [3]). Thus, $R_{\rm eff}$ estimation using equation (3) alone should

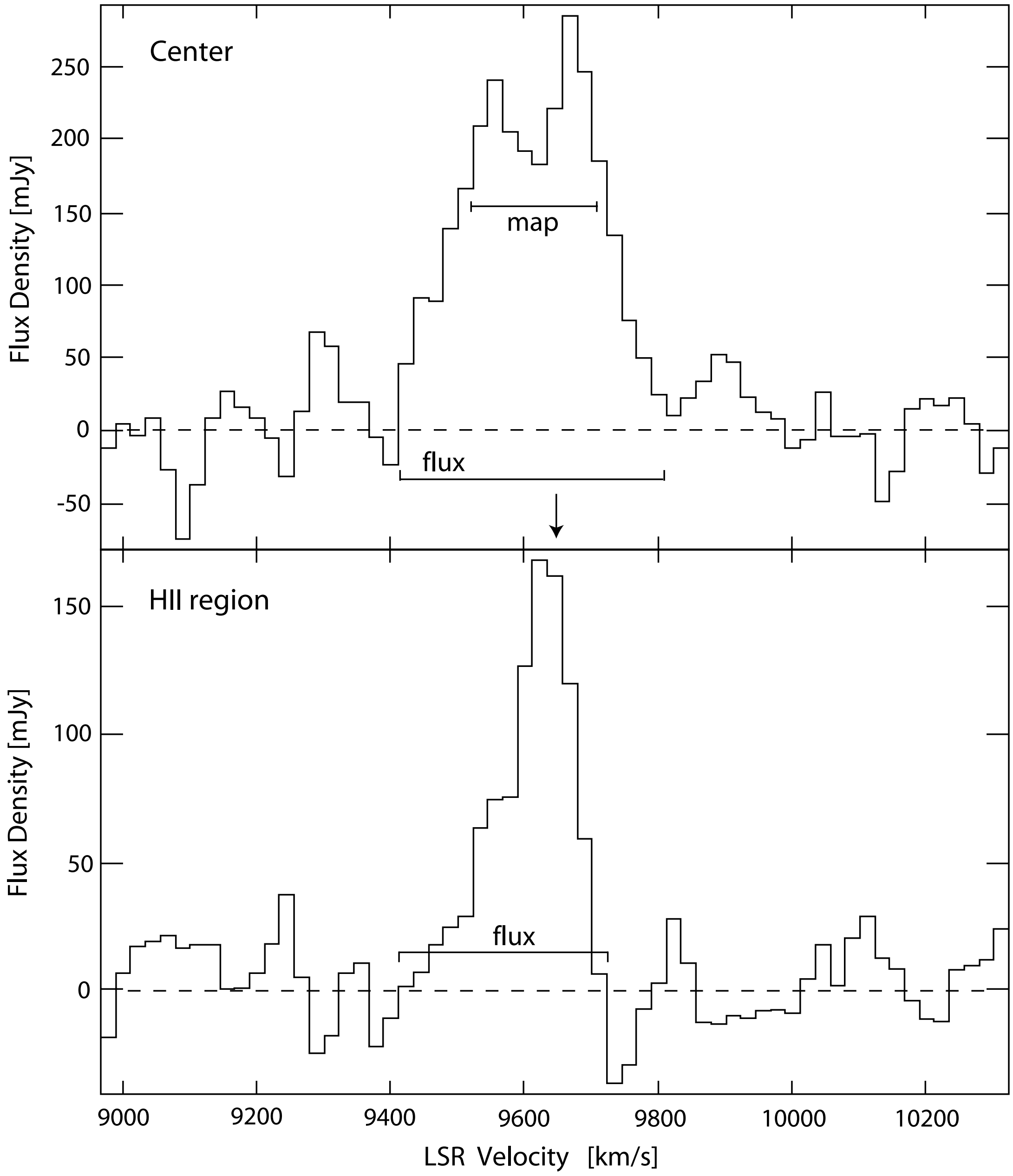

FIG. 4.—Same as Fig. 3, but for IRAS 05262. The top panel shows the spectrum of the central CO gas, while the bottom panel presents the spectrum of the H II region ~7″ south of the center.

not be taken too seriously. For instance, our visual investigation of the radial profile of the two *IRAS* galaxies (data presented by Ohta et al. 2007) lead us to rough estimations of their $R_{\rm eff}$ of $\sim 0.7''$ and $3.1''$ for IRAS 04312 and IRAS 05262, respectively. Because of strong emission from the nuclei, a large uncertainty of $R_{\rm eff}$ evaluated by this method is also inevitable.

For IRAS 04312, the two methods above provide much different estimations (13″ and 1.4″ in diameter). Thus, it is premature to compare these with the extent of the CO gas ($\sim 4'' \times 4''$) and to discuss how much of the total CO flux comes from its bulge region. However, the two values are consistent with each other for IRAS 05262 (7″ and 6″ in diameter). Since the spatial extent of the detected molecular gas in IRAS 05262 ($\sim 5.6'' \times 9.4''$) seems a bit larger than the estimated bulge size, the molecular gas harbored within the bulge would be slightly smaller than the detected $M(H_2)$. To first order, the observed $M(H_2)$ well represents the $M(H_2)$ of the bulge of IRAS 05262. It is unclear whether stars newly born from the molecular gas belong to the bulge or to the galactic disk. In this study, we regard star formation within $R_{\rm eff}$ as bulge growth.

6. MOLECULAR GAS AND BULGE MASSES

Here we compare the molecular gas masses of these two *IRAS* galaxies with the dynamical masses ($M_{\rm dyn}$) and bulge masses ($M_{\rm bulge}$). These masses are summarized in Table 2.

The dynamical mass $M_{\rm dyn}$ is inferred from the CO gas kinematics. We discuss the position-velocity diagrams (Figs. 7 and 8). The enclosed mass $M_{\rm dyn}$ within the central region of IRAS 04312 is 4.1×10^9 $M_\odot$, resulting in a $M(H_2)/M_{\rm dyn}$ ratio of 0.25. For IRAS 05262, $M_{\rm dyn} = 8.0 \times 10^9$ $M_\odot$, and the $M(H_2)/M_{\rm dyn}$ ratio is then 0.35. If we estimate the current stellar mass as $M_{\rm dyn} - M(H_2)$, the molecular gas masses for these two objects account

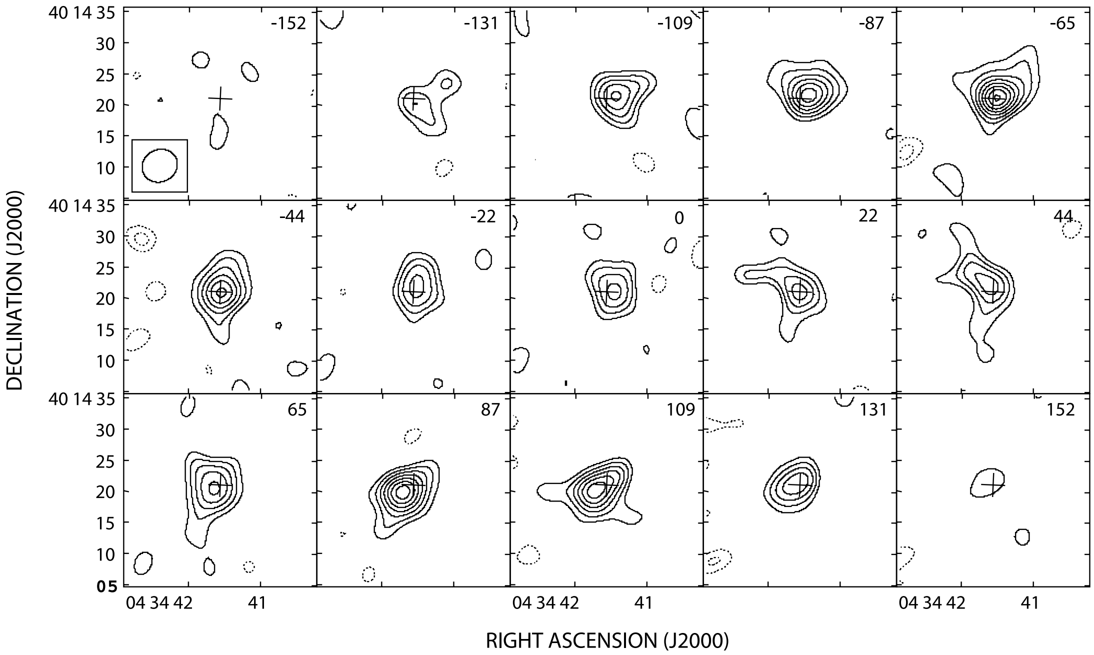

FIG. 5.—CLEANed channel map of the CO(1 $\rightarrow$ 0) emission line around IRAS 04312 over $30'' \times 30''$. Each panel is binned in frequency over 42 km s^{-1}, showing $(-3, -2, 2, 3, 4, 5, \ldots) \times \sigma$ with 1 $\sigma = 19$ mJy beam^{-1} and stepped every 21 km s^{-1}. Crosses represent the peak positions of the full CO emission (Fig. 1). The number in the upper right corner of each panel represents the velocity offset (in km s^{-1}) from the recession velocity of the galaxy (6145 km s^{-1}).

for 33% and 54% of the current stellar masses.[6] However, all the molecular gas will not be consumed by star formation during this star formation episode (in $\sim 10^7$–10^8 yr), since a molecular cloud will be destroyed by photoevaporation, mass loss, and supernova explosion (Williams & McKee 1997). Recycling of the remaining diffuse gas may occur, but on a timescale much longer than the timescale we are considering. Since we are interested in the BH-bulge evolution during one coevolution episode, we do not go further in the recycling process (on a long timescale) in this study. The fraction of molecular gas mass that is converted into stars in molecular clouds (efficiency of star formation) ranges from a few percent (Myers et al. 1986; Wilson & Matthews 1995) to tens of percent (Hillenbrand & Hartmann 1998; Lada & Lada 2003). Adopting a star formation efficiency of 0.1, new stars with masses of 3%–5% of the preexisting stars will be formed in the near future (e.g., within the timescale of cloud destruction, $\sim 10^{7.5}$ yr; Williams & McKee 1997) from the molecular gas.

As we discussed in § 5, the bulge size is not definitively determined. Thus, we cannot be completely sure that the dynamical mass (or virial mass) equals the bulge mass. Therefore, we next try to find another estimation of the bulge mass as a complementary measure. The bulge mass, $M_{\rm bulge}$, can be estimated from the kinematics of stars/clouds embedded in the gravitational potential of the bulge, in the form where $M_{\rm bulge} \propto$ (line width)^4. To determine the normalization in this relationship, we refer to the M-σ_* relationship found in normal galaxies. If we adopt the two

[6] H I gas is normally negligible (compared to H_2 masses) within several kiloparsecs ("molecular front") around galactic centers (Sofue 1994; Sofue & Nakai 1994).

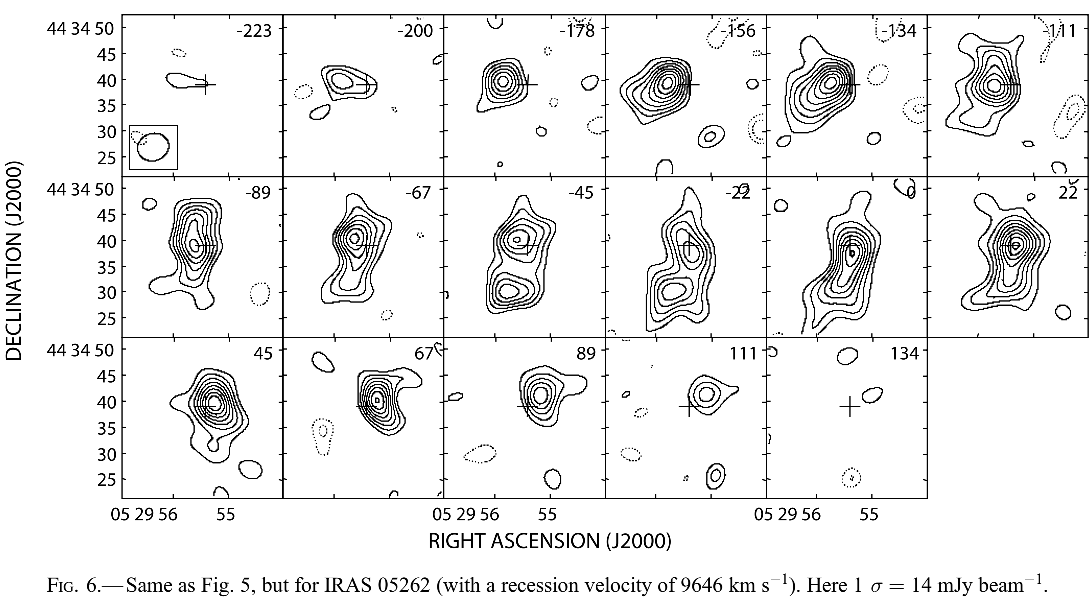

FIG. 6.—Same as Fig. 5, but for IRAS 05262 (with a recession velocity of 9646 km s^{-1}). Here 1 $\sigma = 14$ mJy beam^{-1}.

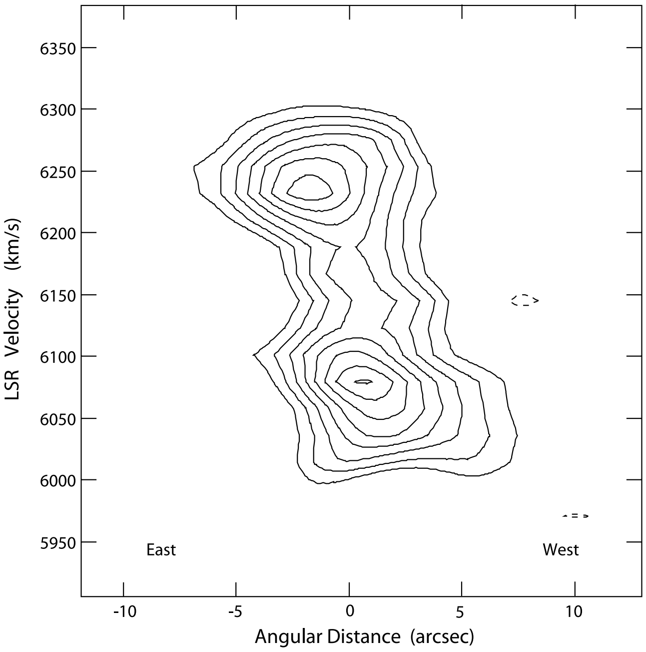

FIG. 7.— Position-velocity diagram of ^{12}CO($1 \rightarrow 0$) emission from IRAS 04312 along a position angle of 108°. The abscissa is the angular distance from the CO emission peak. The contour levels drawn are the same as those of the channel map for the same object (Fig. 5).

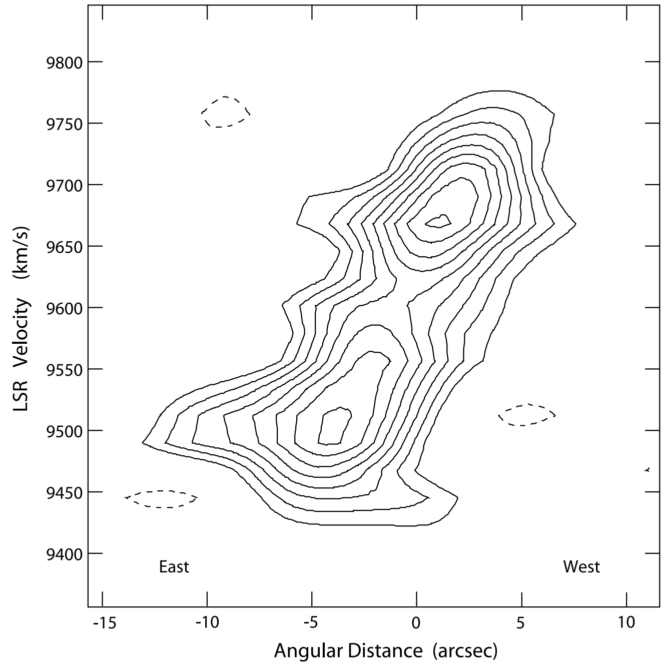

FIG. 8.— Same as Fig. 7, but for IRAS 05262 (with a position angle of 97°).

relations, $M_{\rm BH} = 8 \times 10^6\ M_\odot[\sigma_*/(100\ {\rm km\ s^{-1}})]^4$ and $M_{\rm bulge} = 710 M_{\rm BH}$ (e.g., Tremaine et al. 2002; Gebhardt et al. 2000; Häring & Rix 2004), we obtain the following relationship:

$$M_{\rm bulge} = 5.7 \times 10^9\ M_\odot \left(\frac{\sigma_*}{100\ {\rm km\ s^{-1}}}\right)^4. \quad (4)$$

The scatter in the $M_{\rm BH}$-σ_* relation is about 0.3 dex (Gebhardt et al. 2000), whereas the uncertainty in the $M_{\rm bulge}/M_{\rm BH}$ ratio is also $\sim$0.3 dex (e.g., Marconi & Hunt 2003). The uncertainty of the bulge masses evaluated in this way would thus be about 0.4 dex.

CO widths might be useful to evaluate σ_* and then bulge masses (Shields et al. 2006; Ho 2007; see § 7.2). Here we follow their procedure. Assuming that the dispersion of CO emission-line $\sigma_{\rm CO}$ equals σ_*, as suggested by Shields et al., we adopt $\sigma_{\rm CO}$ of 109 and 110 km s^{-1} for IRAS 04312 and IRAS 05262, respectively (see § 7.2). With equation (4), bulge masses are estimated as $M_{\rm bulge} = 8.0 \times 10^9$ and $8.4 \times 10^9\ M_\odot$, resulting in $M({\rm H_2})/M_{\rm bulge}$ ratios of 0.13 and 0.33, respectively. (If [O III] widths are used as surrogates for σ_* in eq. [4], $M({\rm H_2})/M_{\rm bulge}$ ratios decrease by a factor of 4 [see § 7.2].) Star formation will occur with 1%–3% of the mass of the current stellar masses, for a star formation efficiency of 0.1. Even if we again estimate the mass of preexisting stars by $M_{\rm bulge} - M({\rm H_2})$ to account for the contribution of gas mass, these numbers do not change dramatically.

Let us now summarize this section. The mass of new stars that will be formed (within $\sim 10^{7.5}$ yr from now on) from the molecular gas is not a huge fraction of the current stellar masses (1%–5%). Here we conclude that the bulges of these two NLS1s do not evolve so much in this timescale. If newly born stars are to belong to the galactic disks rather than the bulges, the conclusion (small growth in the bulge mass) is enhanced.

This result can be interpreted in several ways. (1) Coevolution is not simultaneous at all; bulges (and elliptical galaxies) were formed in the early universe (Akiyama 2005; Woo et al. 2006), while BH growth via accretion still happens today. (2) Alternatively, coevolution of BHs and bulges can be (quasi-) simultaneous with two growth episodes overlapped or close in time. (*i*) Our result indicates that the bulge growth finished prior to the BH growth (e.g., Umemura 2001). (*ii*) Or, coevolution may occur intermittently through a number of episodic events. Each coevolving AGN could have very short durations of BH and bulge growth, with small increases in $M_{\rm bulge}$ and $M_{\rm BH}$, resulting in a small fraction of molecular gas associated with the AGN even in the early evolutionary stage (NLS1s). The total lifetime of an AGN is estimated to be $\sim 10^8$ yr (Martini 2004; Jakobsen et al. 2003). However, a lower limit for the duration of an episodic event of an AGN is about 10^4 yr, based on the proximity effect (e.g., Bajtlik et al. 1988) and the sizes of ionization-bounded narrow-line regions (Bennert et al. 2002). Therefore, BH-bulge coevolution could be divided into numerous shorter events.

7. DISCUSSIONS AND SUMMARY

7.1. *Star Formation Rates versus Accretion Rates*

Here we discuss the relation between SFRs and accretion rates and the $M_{\rm bulge}$-$M_{\rm BH}$ relation.

The current SFR can be estimated from FIR luminosity or molecular gas mass. The regression relation between 40–120 μm FIR luminosity[7] and $M({\rm H_2})$ is typically (for galaxies similar to the Milky Way) expressed as (see Kennicutt 1998; Tinney et al. 1990)

$$L_{\rm FIR} = 19 L_\odot \left[\frac{M({\rm H_2})}{M_\odot}\right]. \quad (5)$$

The scatter around this linear relation is about $\pm$0.3 dex (Tinney et al. 1990). (Again, the regression is renormalized here by adopting the same conversion factor we used previously.) Now we estimate the FIR luminosity at each central region (free from the contribution of AGNs) for the two NLS1s, based on their molecular gas masses. (On the other hand, the observed FIR luminosity by *IRAS*, shown below, includes the FIR emission from

[7] $L_{\rm FIR} = 0.65\nu L_\nu(60\ \mu{\rm m}) + 0.42\nu L_\nu(100\ \mu{\rm m})$ (Helou et al. 1985).

TABLE 2
SUMMARY OF VARIOUS MASSES

Object	$M(H_2)$ ($10^9\ M_\odot$)	M_{dyn} ($10^9\ M_\odot$)	Ratio[a]	M_{bulge} ($10^9\ M_\odot$)	Ratio[a]
IRAS 04312	1.0	4.1	0.25	8.0	0.13
IRAS 05262	2.8	8.0	0.35	8.4	0.33

[a] Ratio of the molecular gas masses $M(H_2)$ with respect to the dynamical masses M_{dyn} or bulge masses M_{bulge}.

the entire galaxy and AGNs.) Inferred masses (§ 4.2) indicate that their L_{FIR} values are 1.9×10^{10} and $5.3 \times 10^{10}\ L_\odot$.

By translating these FIR luminosities into the SFR using (Kennicutt 1998)

$$\mathrm{SFR} = 1.7\ M_\odot\ \mathrm{yr}^{-1}\left(\frac{L_{FIR}}{10^{10}\ L_\odot}\right), \tag{6}$$

their SFRs (at the central region) are expected to be 3.3 and 9.2 $M_\odot\ \mathrm{yr}^{-1}$. Most of the normalizations for equation (6) in the literature lie within ±30% for starbursts. Disk galaxies, on average, may have normalization that is a factor of 1.8 higher than equation (6) (Buat & Xu 1996). Taking all the uncertainties of normalizations in equations (5) and (6), an error of SFR estimated from $M(H_2)$ would be $\pm 0.3 + 0.3$ dex.

Incidentally, the observed L_{FIR} values of the two *IRAS* galaxies (measured via *IRAS*, including contributions from an entire host galaxy and nuclei) are $2.7 \times 10^{10}\ L_\odot$ (IRAS 04312) and $6.3 \times 10^{10}\ L_\odot$ (IRAS 05262). If these L_{FIR} values are used instead, their SFRs are evaluated to be 5 and 11 $M_\odot\ \mathrm{yr}^{-1}$, respectively. Since these values likely overestimate the central L_{FIR} and thus central SFRs, we hereafter refer to the SFRs estimated in the previous paragraph.

Next, we evaluate the accretion rates onto their central BHs $\dot{M}$ by adopting two simplified methods. First, we estimate $\dot{M}$ based on bolometric luminosities, with an assumption of constant radiation efficiency. The bolometric luminosity is assumed to be 10 times the optical luminosity, νL_ν(5100 Å) (e.g., Elvis et al. 1994). (We note that up to ~50% of the optical luminosity may originate in the host galaxies [Surace et al. 2001; Bentz et al. 2006]. Thus, the discussion below overestimates $\dot{M}$ by up to a factor of ~2.) The radiation efficiency (with respect to the rest-mass energy of the infalling gas) is set to be 0.05 (e.g., Shakura & Sunyaev 1973; Novikov & Thorne 1973). Then the $\dot{M}$ values are estimated to be 1.3 and 5.2 $M_\odot\ \mathrm{yr}^{-1}$, resulting in SFR/$\dot{M}$ ratios of 2.5 and 1.8 for IRAS 04312 and IRAS 05262, respectively.

When $\dot{M}$ exceeds the Eddington limit ($\sim 16 L_{Edd}/c^2$), however, the radiation efficiency drops due to the onset of photon trapping (Begelman 1978; Abramowicz et al. 1988). Thus, estimates using accretion disk models are better than those using a constant efficiency (see, e.g., Kawaguchi 2003; Collin & Kawaguchi 2004). Here $\dot{M}$ is then estimated based on optical luminosity and the (standard) accretion disk model with a face-on disk geometry assumed (e.g., Bechtold et al. 1987)[8]:

$$\left(\frac{\dot{M}}{M_\odot\ \mathrm{yr}^{-1}}\right) = 2.1\left(\frac{M_{BH}}{10^7\ M_\odot}\right)^{-1}\left[\frac{\nu L_\nu(5100\ \text{Å})}{10^{44}\ \mathrm{erg\ s^{-1}}}\right]^{1.5}. \tag{7}$$

[8] The photon-trapping effect takes place only in the inner part of the disk where UV and soft X-ray photons emerge. In the outer region of the disk, which radiates optical continuum emission, self-gravity (rather than the gravity from the central BH) governs the disk dynamics (Kawaguchi et al. 2004b). Although the standard accretion disk model (Shakura & Sunyaev 1973) works only inside the self-gravity radius, here we adopt the standard disk model beyond the self-gravity radius for the sake of simplicity.

With this equation, we get 19 and 76 $M_\odot\ \mathrm{yr}^{-1}$ for IRAS 04312 and IRAS 05262, respectively. Here we obtain yet smaller SFR/$\dot{M}$ ratios of 0.17 and 0.12, respectively.

Next, let us discuss these ratios in the context of the M_{bulge}-M_{BH} relation. The ratio of bulge masses to BH masses in galaxies is about 700 (Häring & Rix 2004). This number is considerably larger than the SFR-to-$\dot{M}$ ratios for the two NLS1s (~1) estimated above. What does this huge difference mean?

Our result (the SFR-to-$\dot{M}$ ratios ≈1 for the two NLS1s) can indicate that $\dot{M}$ in NLS1s is temporarily large. To compensate for the intense BH growth during the NLS1s, a short-term, intense starburst (with a much higher SFR than the current SFR) happens before or in the future (i.e., bulge growth and BH growth phases appear without an overlapped period). However, if the duration of star formation is much longer than the duration of the AGN phase, such an intense starburst is not required.

7.2. CO *Width as a Surrogate for* σ_*?

Heckman et al. (1989) showed that CO and [O III] lines have similar widths. In addition, [O III] line widths are now often used as surrogates for the bulge stellar dispersion σ_* of AGNs (Nelson & Whittle 1996; Nelson 2000; Shields et al. 2003; Boroson 2003). Then Shields et al. (2006) proposed CO width as a surrogate for σ_* (see also Ho 2007), although they found a systematic difference ($\sigma_{[O\ III]}/\sigma_{CO} \approx 0.15$ dex, on average, for the seven PG quasars they looked at). By using the CO width for high-redshift quasars, they examined the evolution of the M-σ_* relation at $z > 3$, arguing that high-z quasars have smaller M_{bulge}/M_{BH} ratios than quasars at $z < 3$.

Here we compare CO width and [O III] width using our results, in order to assess the relation between CO width and [O III] width for NLS1s. Full width at zero intensity (FWZI) values, evaluated with the ranges shown in Figures 3 and 4 with "flux" labels, for the two NLS1s are 384 km s^{-1} (IRAS 04312) and 388 km s^{-1} (IRAS 05262). Following Shields et al. (2006), we also assume that FWHM(CO) ≈ $\frac{2}{3}$ FWZI. Then FWHM(CO) for these two *IRAS* galaxies is about 260 km s^{-1}, which is less than their FWHM([O III]) widths (380 and 365 km s^{-1}, respectively). This is the same trend that Shields et al. (2006) presented for the PG quasars. Therefore, use of CO width to estimate σ_* can lead to a systematic error on M_{bulge} for NLS1s as well. The difference between the CO and [O III] widths is 0.15–0.17 dex for the two NLS1s, providing a factor of 4 less M_{bulge} for CO-based mass.

7.3. *Summary*

The tight correlation between the mass of the central BHs and the mass of the galactic spheroid components (the galactic bulge or elliptical galaxy itself) in galaxies and AGNs indicates contemporaneous coevolution of the two massive systems. However, no direct evidence for simultaneous growth has been found. We aim to reveal whether BH growth and bulge growth take place (quasi-) simultaneously by determining the amount and distribution of molecular gas (fuel for the coming star formation) in young AGNs.

NLS1s are characterized by relatively small BH masses and high Eddington ratios. Larger $\dot{M}/M_{\rm BH}$ ratios of NLS1s than of BLS1s indicate that BHs in NLS1s are growing rapidly and that NLS1s are younger than BLS1s. If the growth phases of BHs and bulges are really overlapped, bulges of NLS1s may also be rapidly growing with a significant amount of molecular gas accumulated in their bulges. However, NLS1s are only 10%–30% of Seyfert 1 galaxies, and thus we do not have many NLS1s whose CO emission is detected in the nearby universe. In order to investigate the nature of molecular gas in NLS1s in general, it is of fundamental importance to increase the number of nearby NLS1s with CO emission lines detected.

Thus, we perform ^{12}CO($1 \rightarrow 0$) observations using the NMA D configuration for two FIR-bright NLS1s located at $z = 0.020-0.032$ with $5''$–$6''$ (2–4 kpc at their distance) resolution. We detect their CO emission for the first time, with $M({\rm H_2})$ of $(1–3) \times 10^9\ M_\odot$. These molecular gas masses are the second and fourth largest masses among NLS1s.

By estimating $M_{\rm dyn}$ and $M_{\rm bulge}$ with the CO channel maps and CO line widths, we get $M({\rm H_2})/M_{\rm dyn}$ and $M({\rm H_2})/M_{\rm bulge}$ ratios of 0.25–0.35 and 0.13–0.33, respectively. Taking into account the star formation efficiency (∼0.1), the increase in $M_{\rm bulge}$ in those NLS1s in the near future is not expected to be a huge fraction (1%–5% of the mass of the preexisting stars). This result can be interpreted in several ways. Coevolution may not be simultaneous at all; bulges (and elliptical galaxies) were formed in the early universe, while BH growth via accretion still happens today. Or, the bulge growth may have finished prior to the BH growth. Alternatively, coevolution may proceed with many occasional discrete events, where one coevolution event produces only a small amount of mass growth of BHs and bulges.

We further discuss the relation between SFRs and accretion rates in the context of the $M_{\rm BH}$-$M_{\rm bulge}$ correlation. The two NLS1s turned out to have much smaller SFR/$\dot{M}$ ratios (≈1) than the $M_{\rm bulge}/M_{\rm BH}$ ratios of normal and active galaxies. This huge difference can indicate either that bulge growth and BH growth phases appear without an overlapped period, or that the duration of star formation is much larger than the duration of the AGN phase.

For the two NLS1s, the CO widths are less than the [O III] widths (by 0.15–0.17 dex), which is the same trend that Shields et al. (2006) presented for several PG quasars. Therefore, use of CO width to estimate σ_* can lead to a systematic error (a factor of 4 less mass) on $M_{\rm bulge}$ for NLS1s as well.

We thank the NMA staff for helping with the observations. This research has made use of the NASA/IPAC Extragalactic Database (NED), which is operated by the Jet Propulsion Laboratory, California Institute of Technology, under contract with the National Aeronautics and Space Administration. T. K. is grateful for the financial support from a Grant-in-Aid for Scientific Research of JSPS (18840038) and from the Research Institute of Aoyama Gakuin University. The Nobeyama Radio Observatory is a branch of the National Astronomical Observatory of Japan, the National Institutes of Natural Sciences (NINS).

REFERENCES

Abramowicz, M. A., Czerny, B., Lasota, J. P., & Szuszkiewicz, E. 1988, ApJ, 332, 646
Akiyama, M. 2005, ApJ, 629, 72
Bajtlik, S., Duncan, R. C., & Ostriker, J. P. 1988, ApJ, 327, 570
Bechtold, J., Czerny, B., Elvis, M., Fabbiano, G., & Green, R. F. 1987, ApJ, 314, 699
Begelman, M. C. 1978, MNRAS, 184, 53
Bennert, N., Falcke, H., Schulz, H., Wilson, A. S., & Wills, B. J. 2002, ApJ, 574, L105
Bentz, M. C., Peterson, B. M., Pogge, R. W., Vestergaard, M., & Onken, C. A. 2006, ApJ, 644, 133
Boller, Th., Brandt, W. N., Fabian, A. C., & Fink, H. H. 1997, MNRAS, 289, 393
Boller, Th., Brandt, W. N., & Fink, H. H. 1996, A&A, 305, 53
Boroson, T. A. 2003, ApJ, 585, 647
Borys, C., Smail, I., Chapman, S. C., Blain, A. W., Alexander, D. M., & Ivison, R. J. 2005, ApJ, 635, 853
Botte, V., Ciroi, S., Rafanelli, P., & Di Mille, F. 2004, AJ, 127, 3168
Brandt, W. N., & Boller, T. 1998, in AIP Conf. Ser. 431, Accretion Processes in Astrophysical Systems: Some Like It Hot!, ed. S. S. Holt & T. R. Kallman (Melville: AIP), 191
Buat, V., & Xu, C. 1996, A&A, 306, 61
Collin, S., & Kawaguchi, T. 2004, A&A, 426, 797
Collin, S., Kawaguchi, T., Peterson, B. M., & Vestergaard, M. 2006, A&A, 456, 75
Dame, T. M., Hartmann, D., & Thaddeus, P. 2001, ApJ, 547, 792
Downes, D., & Solomon, P. M. 1998, ApJ, 507, 615
Elvis, M., et al. 1994, ApJS, 95, 1
Evans, A. S., Frayer, D. T., Surace, J. A., & Sanders, D. B. 2001, AJ, 121, 3285
Ferrarese, L., & Merritt, D. 2000, ApJ, 539, L9
Gebhardt, K., et al. 2000, ApJ, 539, L13
Guzman, R., Lucey, J. R., & Bower, R. G. 1993, MNRAS, 265, 731
Halpern, J. P., & Oke, J. B. 1987, ApJ, 312, 91
Häring, N., & Rix, H.-W. 2004, ApJ, 604, L89
Hayashida, K. 2000, NewA Rev., 44, 419
Heckman, T. M., Blitz, L., Wilson, A. S., Armus, L., & Miley, G. K. 1989, ApJ, 342, 735
Helou, G., Soifer, B. T., & Rowan-Robinson, M. 1985, ApJ, 298, L7
Hillenbrand, L. A., & Hartmann, L. W. 1998, ApJ, 492, 540
Ho, L. C. 2007, ApJ, 669, 821
Jakobsen, P., Jansen, R. A., Wagner, S., & Reimers, D. 2003, A&A, 397, 891
Kaspi, S., Maoz, D., Netzer, H., Peterson, B. M., Vestergaard, M., & Jannuzi, B. T. 2005, ApJ, 629, 61
Kaspi, S., Smith, P. S., Netzer, H., Maoz, D., Jannuzi, B. T., & Giveon, U. 2000, ApJ, 533, 631
Kauffmann, G., & Haehnelt, M. 2000, MNRAS, 311, 576
Kauffmann, G., White, S. D. M., & Guiderdoni, B. 1993, MNRAS, 264, 201
Kawaguchi, T. 2003, ApJ, 593, 69
Kawaguchi, T., Aoki, K., Ohta, K., & Collin, S. 2004a, A&A, 420, L23
Kawaguchi, T., Pierens, A., & Huré, J.-M. 2004b, A&A, 415, 47
Kennicutt, R. C., Jr. 1998, ARA&A, 36, 189
Kiuchi, G., Ohta, K., Akiyama, M., Aoki, K., & Ueda, Y. 2006, ApJ, 647, 892
Kohno, K., Kawabe, R., Ishizuki, S., & Vila-Vilaró, B. 1999a, Adv. Space Res., 23, 1011
Kohno, K., Kawabe, R., & Vila-Vilaró, B. 1999b, in The Physics and Chemistry of the Interstellar Medium, ed. V. Ossenkopf, J. Stutzki, & G. Winnewisser (Herdecke: GCA), 34
Komossa, S., & Xu, D. 2007, ApJ, 667, L33
Lada, C. J., & Lada, E. A. 2003, ARA&A, 41, 57
Laor, A., Fiore, F., Elvis, M., Wikes, B. J., & McDowell, J. C. 1997, ApJ, 477, 93
Leighly, K. M. 1999a, ApJS, 125, 297
———. 1999b, ApJS, 125, 317
Maiolino, R., Ruiz, M., Rieke, G. H., & Papadopoulos, P. 1997, ApJ, 485, 552
Marconi, A., & Hunt, L. K. 2003, ApJ, 589, L21
Martini, P. 2004, in Coevolution of Black Holes and Galaxies, ed. L. C. Ho (Cambridge: Cambridge Univ. Press), 169
Mathur, S. 2000, MNRAS, 314, L17
Mineshige, S., Kawaguchi, T., Takeuchi, M., & Hayashida, K. 2000, PASJ, 52, 499
Myers, P. C., Dame, T. M., Thaddeus, P., Cohen, R. S., Silverberg, R. F., Dwek, E., & Hauser, M. G. 1986, ApJ, 301, 398
Nelson, C. H. 2000, ApJ, 544, L91
Nelson, C. H., & Whittle, M. 1996, ApJ, 465, 96
Novikov, I. D., & Thorne, K. S. 1973, in Black Holes, ed. C. De Witt & B. De Witt (New York: Gordon & Breach), 343
Ohta, K., Aoki, K., Kawaguchi, T., & Kiuchi, G. 2007, ApJS, 169, 1
Okumura, S. K., et al. 2000, PASJ, 52, 393
Onken, C. A., Ferrarese, L., Merritt, D., Peterson, B. M., Pogge, R. W., Vestergaard, M., & Wandel, A. 2004, ApJ, 615, 645
Osterbrock, D. E., & Pogge, R. W. 1985, ApJ, 297, 166
Otani, C., Kii, T., & Miya, K. 1996, in Int. Conf. X-Ray Astronomy and Astrophysics: Röntgenstrahlung from the Universe, ed. H. U. Zimmermann, J. E. Trümper, & H. Yorke (Garching: MPE Press), 491

Paturel, G., Theureau, G., Bottinelli, L., Gouguenheim, L., Coudreau-Durand, N., Hallet, N., & Petit, C. 2003, A&A, 412, 57
Pogge, R. W. 2000, NewA Rev., 44, 381
Pounds, K. A., Done, C., & Osborne, J. 1995, MNRAS, 277, L5
Rees, M. J. 1992, in Physics of Active Galactic Nuclei, ed. W. J. Duschl & S. J. Wagner (Berlin: Springer), 662
Shakura, N. I., & Sunyaev, R. A. 1973, A&A, 24, 337
Shields, G. A., Gebhardt, K., Salviander, S., Wills, B. J., Xie, B., Brotherton, M. S., Yuan, J., & Dietrich, M. 2003, ApJ, 583, 124
Shields, G. A., Menezes, K. L., Massart, C. A., & Vanden Bout, P. 2006, ApJ, 641, 683
Silk, J., & Rees, M. 1998, A&A, 331, L1
Sofue, Y. 1994, PASJ, 46, 173
Sofue, Y., & Nakai, N. 1994, PASJ, 46, 147
Solomon, P. M., Downes, D., Radford, S. J. E., & Barrett, J. W. 1997, ApJ, 478, 144
Surace, J. A., Sanders, D. B., & Evans, A. S. 2001, AJ, 122, 2791
Taniguchi, Y., Kameya, O., Nakai, N., & Kawara, K. 1990, ApJ, 358, 132
Tinney, C. G., Scoville, N. Z., Sanders, D. B., & Soifer, B. T. 1990, ApJ, 362, 473
Tremaine, S., et al. 2002, ApJ, 574, 740
Tsutsumi, T., Morita, K.-I., & Umeyama, S. 1997, in ASP Conf. Ser. 125, Astronomical Data Analysis Software and Systems VI, ed. G. Hunt & H. E. Payne (San Francisco: ASP), 50
Umemura, M. 2001, ApJ, 560, L29
Véron-Cetty, M. P., Véron, P., & Gonçalves, A. C. 2001, A&A, 372, 730
Wandel, A., Peterson, B. M., & Malkan, M. A. 1999, ApJ, 526, 579
Wang, T., Brinkmann, W., & Bergeron, J. 1996, A&A, 309, 81
Williams, J. P., & McKee, C. F. 1997, ApJ, 476, 166
Wilson, C. D., & Matthews, B. C. 1995, ApJ, 455, 125
Woo, J.-H., Treu, T., Malkan, M. A., & Blandford, R. D. 2006, ApJ, 645, 900
Young, J. S., et al. 1995, ApJS, 98, 219